2026 JULY 19–22 VANCOUVER, BC
JOINT AAPM | COMP MEETING
MEDICAL PHYSICS COMMUNITY · INSPIRATION · INNOVATION · IMPACT

Collimator and detector optimization for Compton scatter detection: a first step towards scatter imaging for real-time motion management in lung SBRT

N Lowther, M Myronakis, T Harris, R Berbeco, F De Kermenguy, M Jacobson, R Etemadpour, B Vecchione, D Ferguson, YH Hu

Department of Radiation Oncology, Brigham and Women's Hospital, Dana-Farber Cancer Institute, Harvard Medical School, Boston, MA.

Introduction

- Existing real-time tracking methods during lung SBRT require implanted fiducials or additional imaging dose. A non-invasive, dose-free method for real-time tumor tracking is warranted.
- Passive detection of Compton-scattered, therapeutic photons may offer a novel solution (*Figure 1*).

Methods and Materials

- The GEANT4 GATE MC toolkit, which allows accurate scintillation system modelling, was utilized.
- Phase-space analyses first determined the optimal scatter angle of scattered photons (SPs) that preserved phantom geometry in a scatter image, for a clinical 6 MV FFF beam.
- To translate the findings of the phase-space analysis into a physical detector (*Figure 2*), position, scintillation material, and collimator properties: septal height (*H*), thickness (*T*), interspace (*I*), and material of parallel-focused 2D collimator grids (CGs) were varied
- The angular detection significance metric (ADSM), defined as the number of detected SPs within the optimal scatter angle divided by the square root of the total detected photons, served as the performance metric.

Results

- Mean photon energies increased from 0.18 MeV at 45° to 0.27 MeV at 90° and 0.52 MeV at 135° (*Figure 3*), with the latter exhibiting a pronounced high-energy tail.
- Progressive restriction of the scatter angle markedly improved reconstructed image quality, with an acceptance range of ±0.5° producing an image that closely reproduced the known phantom geometry (*Figure 4*).
- Phase-space analysis further demonstrated that multiply scattered photons contributed meaningful image signal (*Figure 5*)
- The detector configuration with highest ADSM, 54.38, (*Table 1*) was then used to create scatter images of an anthropomorphic phantom for a 5 x 5 cm open field with a clinical 6 MV FFF beam for a 5.8 MU exposure (~4 fps equivalent imaging). Pixel array size and filters were varied (*Figure 6*)

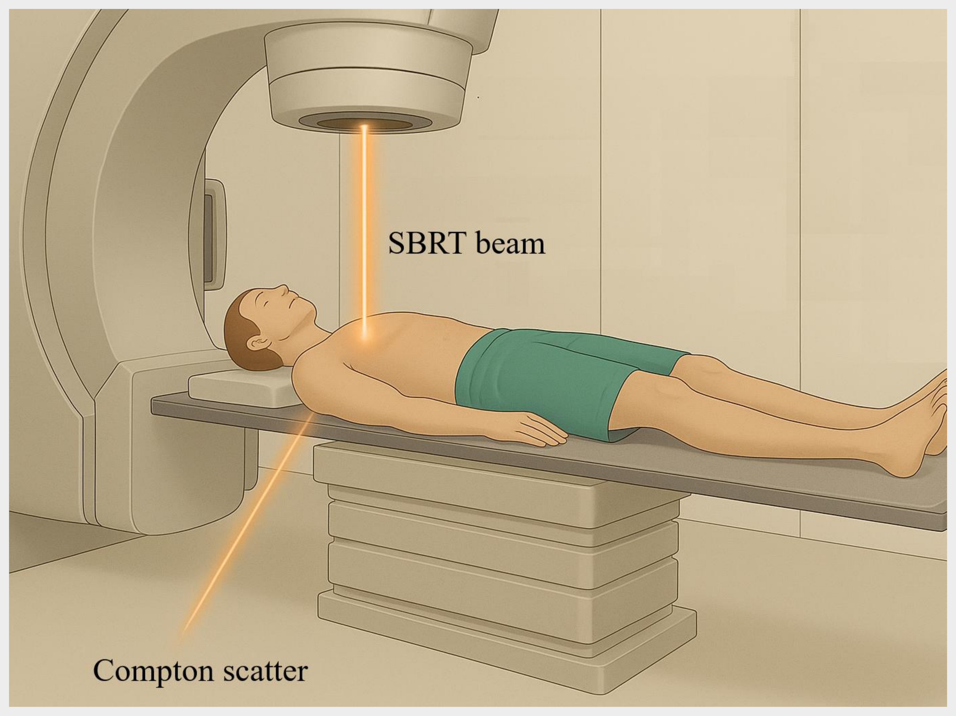

Figure 1: *Simplistic example of a Compton scatter photon. This work used Monte Carlo to vary collimators and detectors, and their geometric positioning in effort to design an optimal detector for passive scatter imaging.*

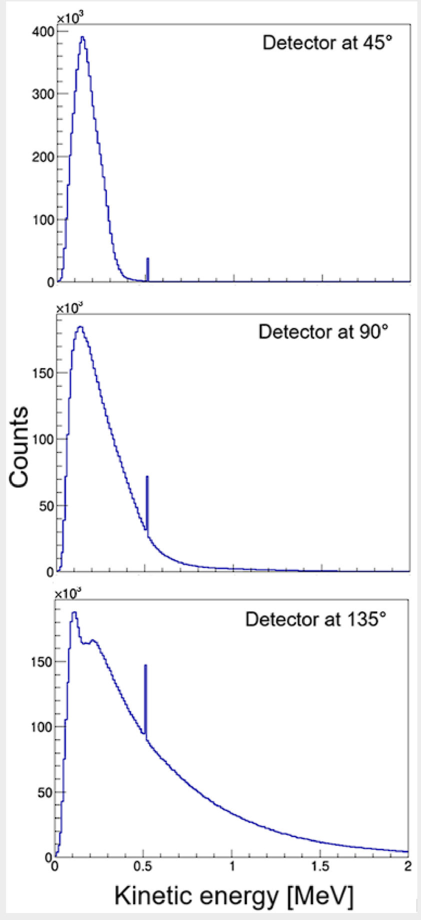

Figure 3 (left): *Resultant kinetic energy spectra of scattered photons for a phase-space volume positioned at 45°, 90° and 135° all at 50 cm from isocenter.*

Figure 4 (right): *Further phase-space results and interpretation aids. The 3D scatter cone demonstrates the phi and theta angles for SPs for an MV treatment beam irradiating a phantom at isocenter (i.e., 0,0,0). Digital phantom used for the MC simulations (bot left). The phase-space analysis showed that progressive constriction (a-d) of the SPs' phi and theta angles resulted in a geometrically accurate image of the phantom when the angles were limited to ±0.5° (e). This 'detector' phase-space volume was placed at 50 cm from the isocenter at 90° to the incident MV beam. A 10 x 10 cm open field with a clinical 6 MV FFF beam of ~0.7 MU was used..*

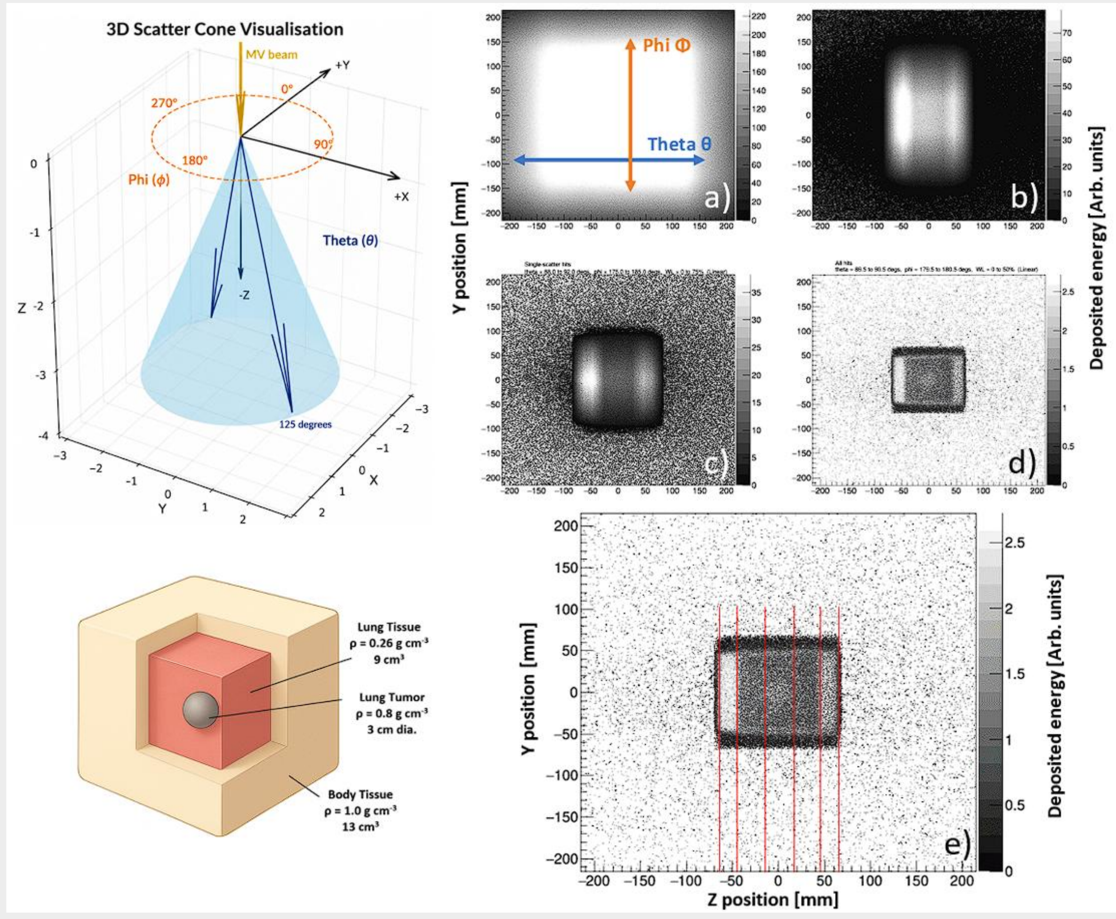

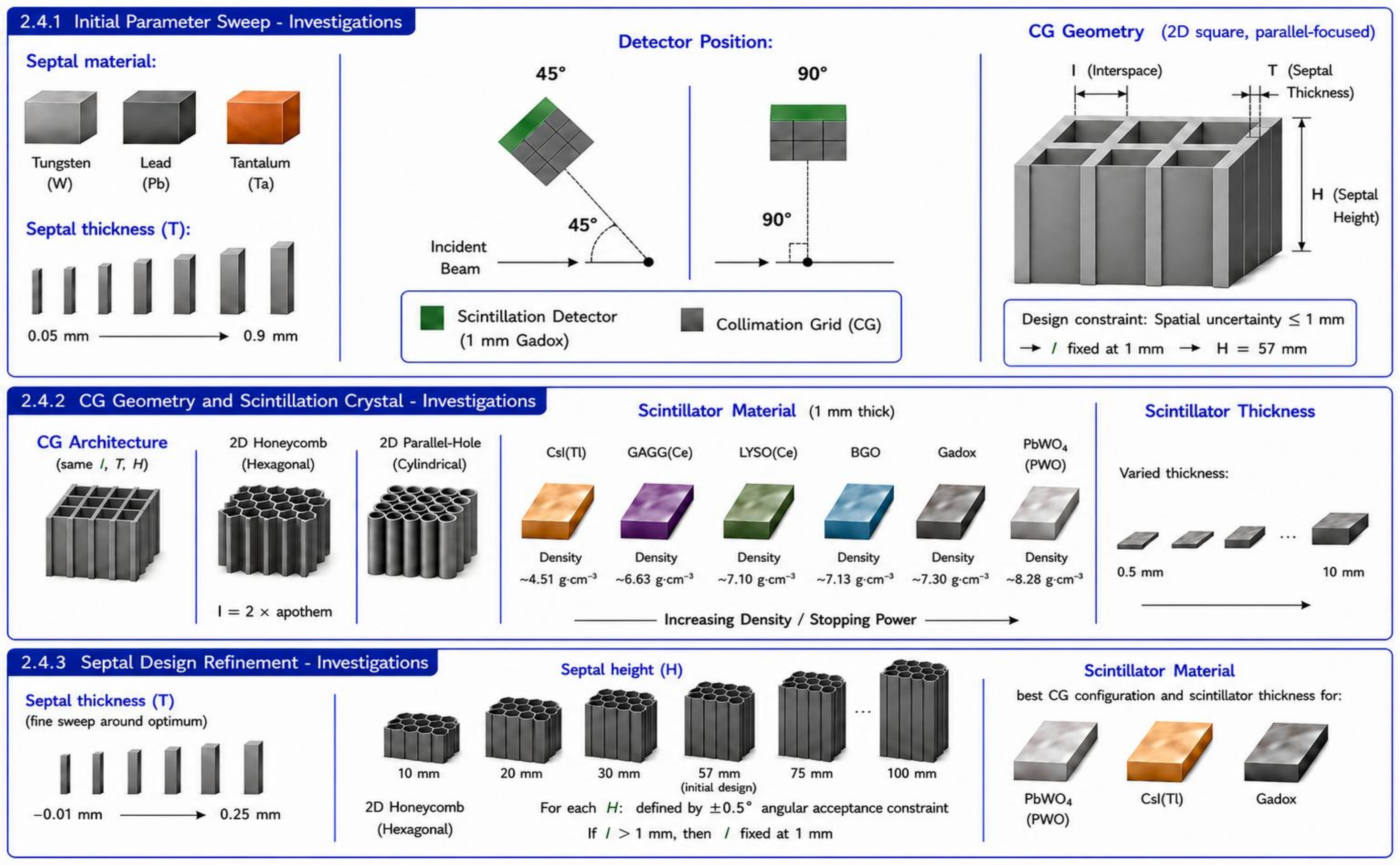

Figure 2: *Overview of the staged investigation and optimization framework followed to digitally reproduce the collimation of the phase-space analysis on a physical detector towards optimal Compton scatter detector design.*

Table 1*: A summary of the ADSM results for a sample of the simulated detector positions, collimation grid (CG) configurations and scintillation crystal properties.*

Detector angle	H [mm]	T [mm]	I [mm]	Scin. crystal	Crystal thickness [mm]	CG shape	CG material	ADSM
90°	57	0.05	1.0	Gadox	1.0	Square	Tungsten	12.24
90°	57	0.1	1.0	Gadox	1.0	Square	Tantalum	15.64
45°	57	0.3	1.0	Gadox	1.0	Square	Tantalum	28.41
90°	57	0.3	1.0	Gadox	1.0	Square	Lead	20.22
45°	57	0.1	1.0	Gadox	1.0	Square	Lead	29.76
45°	57	0.1	1.0	Gadox	1.0	Cylinder	Tungsten	33.09
45°	57	0.1	1.0	Gadox	1.0	HoneyComb	Tungsten	34.52
45°	57	0.1	1.0	Gadox	1.0	Square	Tungsten	33.73
45°	57	0.1	1.0	CSI	1.0	HoneyComb	Tungsten	27.53
45°	57	0.1	1.0	BGO	1.0	HoneyComb	Tungsten	39.64
45°	57	0.1	1.0	GAGG	1.0	HoneyComb	Tungsten	13.61
45°	57	0.1	1.0	LYSO	1.0	HoneyComb	Tungsten	19.03
45°	57	0.1	1.0	PWO	3.0	HoneyComb	Tungsten	50.21
45°	57	0.1	1.0	PWO	3.5	HoneyComb	Tungsten	50.68
45°	57	0.1	1.0	PWO	4.0	HoneyComb	Tungsten	50.20
45°	57	0.1	1.0	CSI(Tl)	9.0	HoneyComb	Tungsten	41.47
45°	57	0.1	1.0	CSI(Tl)	12.0	HoneyComb	Tungsten	40.80
45°	57	0.1	1.0	Gadox	5.0	HoneyComb	Tungsten	43.69
45°	57	0.1	1.0	Gadox	5.5	HoneyComb	Tungsten	44.37
45°	57	0.1	1.0	Gadox	6.0	HoneyComb	Tungsten	43.42
45°	10	0.2	0.175	PWO	3.5	HoneyComb	Tungsten	19.38
45°	**75**	**0.15**	**1.0**	**PWO**	**3.5**	**HoneyComb**	**Tungsten**	**54.38**
45°	100	0.025	1.0	PWO	3.5	HoneyComb	Tungsten	21.01
45°	57	0.15	1.0	CSI	9.0	HoneyComb	Tungsten	42.47
45°	75	0.2	1.0	CSI	9.0	HoneyComb	Tungsten	40.45
45°	75	0.15	1.0	CSI	9.0	HoneyComb	Tungsten	42.70
45°	100	0.01	1.0	CSI	9.0	HoneyComb	Tungsten	7.82
45°	10	0.3	0.175	Gadox	5.5	HoneyComb	Tungsten	14.96
45°	30	0.1	0.52	Gadox	5.5	HoneyComb	Tungsten	36.17
45°	57	0.1	1.0	Gadox	5.5	HoneyComb	Tungsten	44.37
45°	75	0.1	1.0	Gadox	5.5	HoneyComb	Tungsten	47.60
45°	100	0.1	1.0	Gadox	5.5	HoneyComb	Tungsten	42.03

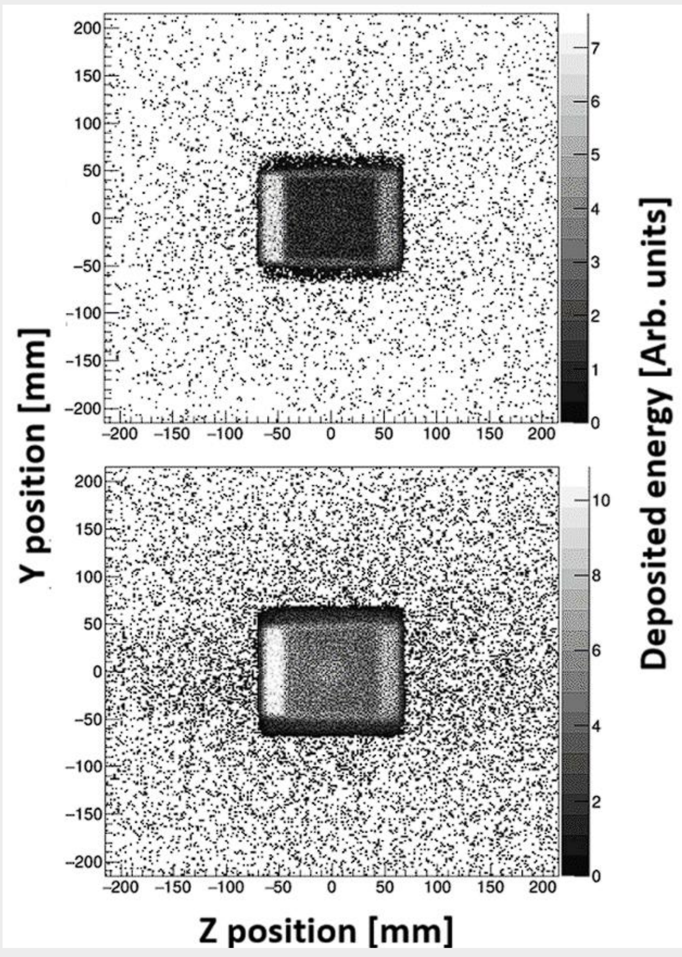

Figure 5: *Image from single-SPs only (top) and for all SPs (bot) within ± 0.5°. For a detector positioned at 90 degrees, 50 cm from isocenter.*

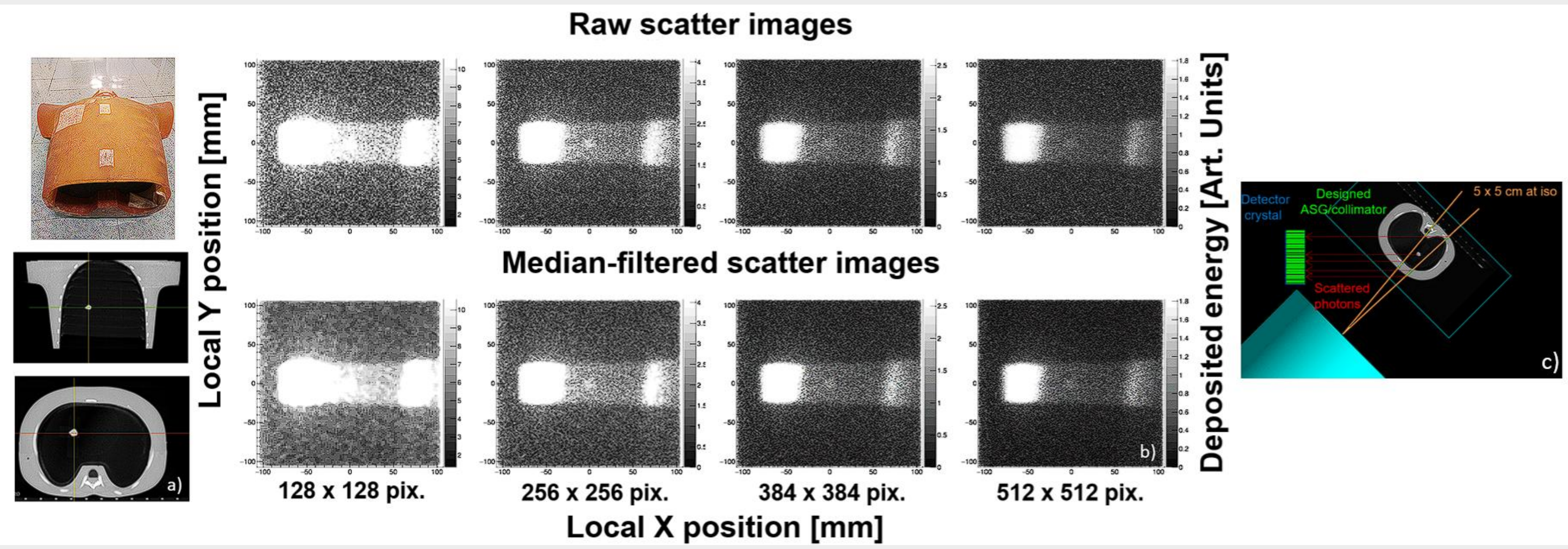

Figure 6: *Photo and CBCT coronal and axial planes of the anthropomorphic phantom used in the MC simulations, cross hairs on the tumor (a). Compton scatter images for varied pixel arrays showing the tumor at 0,0 (b). Visual representation of the final scatter imaging geometry. The detector images obliquely at a 45° angle, close to the treatment head (c).*

DISCUSSION & CONCLUSIONS

- A comprehensive MC optimization framework identified a 45° detector position combined with a honeycomb tungsten collimator as the most effective configuration for passive detection and imaging of Compton-scattered, therapeutic photons during lung SBRT
- These findings establish a practical design foundation for the development of passive Compton scatter imaging systems which may be capable of supporting non-invasive, dose-free real-time motion monitoring during lung SBRT, warranting future refinement, experimental validation and dynamic tracking studies

Nicholas Lowther, PhD
Department of Radiation Oncology, Brigham and Women's Hospital, Dana-Farber Cancer Institute, Harvard Medical School, Boston, MA.
nlowther@bwh.harvard.edu

QR

Connect and flick me and email!

HARVARD MEDICAL SCHOOL